

## High-pressure dc magnetic measurements on a bisdiselenazoly radical ferromagnet using a vibrating-coil SQUID magnetometer

Kunihiko Irie,<sup>1</sup> Keisuke Shibayama,<sup>1</sup> Masaki Mito,<sup>1,\*</sup> Seishi Takagi,<sup>1</sup> Mamoru Ishizuka,<sup>2</sup>  
Kristina Lekin,<sup>3</sup> and Richard T. Oakley<sup>3</sup>

<sup>1</sup>Graduate School of Engineering, Kyushu Institute of Technology, Kitakyushu 804-8550, Japan

<sup>2</sup>Center for Scientific Instrument Renovation and Manufacturing Support, Osaka University, Toyonaka 560-8531, Japan

<sup>3</sup>Department of Chemistry, University of Waterloo, Waterloo, Ontario, Canada N2L 3G1



(Received 21 November 2018; revised manuscript received 30 December 2018; published 17 January 2019)

The high-pressure magnetic properties of the iodo-substituted bisdiselenazoly radical ferromagnet IBPSSEt have been studied by vibrating-coil SQUID magnetometry. The magnetic state at a pressure ( $P$ ) of approximately 2 GPa has the highest Curie temperature ( $T_C$ ) of 27.5 K, and displays an ideal three-dimensional (3D) ferromagnetic interaction network. The value of  $T_C$  observed by ac magnetic susceptibility measurements is consistent with that obtained from dc measurements below approximately 4 GPa. Field-cooled dc measurements at more elevated pressures reveal a slow evolution of magnetic ordering, so that at  $P > 6$  GPa the structure may be described in terms of a 1D ferromagnetic chain with predominantly antiferromagnetic lateral (interchain) interactions, in accord with the results of density functional theory calculations.

DOI: [10.1103/PhysRevB.99.014417](https://doi.org/10.1103/PhysRevB.99.014417)

### I. INTRODUCTION

In 1963, Anderson noted the potential of “crystals of organic free radicals” as a new category of magnetic material [1]. Since then the idea that molecular radicals might serve as building blocks for organic ferromagnets has stimulated research in the design of new radical-based magnetic materials [2–6]. The study of ferromagnetic exchange interactions in radical systems started with the study of galvinoxyl in 1967 [7,8] and bulk ferromagnetic (FM) ordering by a through-bond interaction was observed for the first time in the  $\beta$ -phase of  $p$ -nitrophenyl nitronyl nitroxide ( $p$ -NPNN) in 1991 [9]. Later, many other light heteroatom radicals such as nitroxyls and verdazyls displaying ferromagnetic order (FMO) were characterized [10–13]. Ferromagnetic thiazyl radicals [14] and radical ions [15] have also been generated. In the latter systems the value of  $T_C$  (7 K) can be increased to more than 10 K by the application of pressure [16]. Later work on a mixed bis(thiaselenazoly) radical containing two sulfur and two selenium atoms afforded  $T_C = 12$  K [17], and with full selenium incorporation  $T_C$  was raised to 17 K [18]. This latter value exceeds the highest value previously observed for non-metal-based ferromagnets (16 K for TDAE · C<sub>60</sub> in 1991) [19]. The effect of pressure on the structure and magnetic properties of these high  $T_C$  materials has deepened our understanding of their magnetic interaction networks [20–22].

Along with systematic structural modifications by syntheses (chemical pressure), the use of hydrostatic physical pressure to control and modify molecular crystal structures has proven an effective means of increasing  $T_C$  [5]. As shown

in Table I and Fig. 1, the change in  $T_C$  as a function of pressure ( $P$ ) has been investigated for many radical ferromagnets, including galvinoxyl [23,24],  $\beta$ -phase  $p$ -NPNN [25–27] and other nitronyl nitroxides [28], Dupeyredioxyl [29], TEMPO [30], as well as various verdazyl, thiazyl [5,16], and selenazyl [20–22,31] systems. For some radicals FM ordering has been observed to evolve to antiferromagnetic (AFM) ordering at high pressures, i.e., an FM-to-AFM transition [5,26,27,30]. Among them,  $p$ -Cl-TEMPO with intermolecular C–H ··· O–N contacts exhibits repeated down-up changes in  $T_C$  accompanying a systematic reduction in the magnitude of the magnetic susceptibility [30]. Indeed, all radical ferromagnets eventually lose bulk FM ordering with increasing compression to higher pressures, as it is difficult to maintain a ferromagnetic correlation for all interaction paths, given the  $\pi$ -stacked architecture found in most radical crystal structures and their nonlocalized molecular spin distribution.

Understanding the response of bisdiselenazoly radical ferromagnets XBPSSEt ( $X = \text{Cl, Br, I}$ ) to pressure has been aided by the use of density functional theory broken symmetry (DFT-BS) methods to explore variations in the sign and magnitude of exchange interactions along and between the herringbone arrays of radical  $\pi$ -stacks, as shown in Fig. 2. The chlorine- and bromine-substituted derivatives ( $X = \text{Cl, Br}$ ) both have  $T_C$  near 17 K at ambient pressure, values which increase up to 21 and 24 K, respectively, with applied pressure (Fig. 1) [20,21]. The main reason for the increase in  $T_C$  has been interpreted in terms of an initial FM ( $+ve$ ) enhancement in the exchange interaction  $J_\pi$  between adjacent radicals along the slipped  $\pi$ -stack arrays. However, with increasing  $\pi$ -stack slippage occasioned by higher pressures, this exchange interaction becomes antiferromagnetic ( $-ve$ ). More recent ac measurements on the corresponding iodo-substituted derivative IBPSSEt revealed an ambient pressure  $T_C$  which increased rapidly to 27.5 K at around  $P = 2$  GPa,

\*mitoh@mns.kyutech.ac.jp

TABLE I. Pressure dependence of  $T_C$  for radical ferromagnets.  $\beta$ -*p*-NPNN:  $\beta$ -phase *para*-nitrophenyl nitronyl nitroxide ( $C_{13}H_{16}N_3O_4$ ), *p*-Cl-TEMPO: 4-(*p*-chlorobenzylideneamino)-2,2,6,6-tetramethylpiperidin-1-yloxy ( $C_{16}H_{22}ClN_2O$ ), 2,5-DFPNN: 2,5-difluorophenyl- $\alpha$ -nitronyl nitroxide ( $C_{13}H_{15}N_2O_2F_2$ ), Dupeyredioxyl: *N,N'*-dioxyl-1,3,5,7-tetramethyl-2,6-diazaadamantane,  $\gamma$ -BBDTA  $\cdot$  GaCl<sub>4</sub>:benzo[1,2-*d*:4,5-*d'*]bis[1,3,2]dithiazole  $\cdot$  GaCl<sub>4</sub>, ClBPSSEt: 8-Chloro-4-ethyl-4H-bis[1,2,3]diselenazolo[4,5-*b*:5',4'-*e*]pyridin-3-yl ( $C_7H_5ClN_3Se_4$ ), BrBPSSEt:  $C_7H_5BrN_3Se_4$ , IBPSSEt:  $C_7H_5IN_3Se_4$ .  $P_0$  signifies  $P = 0$  and  $P_c$  is the critical pressure for FM-to-AFM transition, as determined by  $M$ - $H_{dc}$  measurements.

No.	Radical ferromagnet	Category	Initial $T_C(P_0)$ (K)	Initial $dT_C/dP$ (K/GPa)	$d\{T_C/T_C(P_0)\}/dP$ (/GPa)	Maximum $T_C$ (K)	$P_c$ (GPa)	Year	Ref.
1	$\beta$ - <i>p</i> -NPNN	Nitroxyl	0.61	$-2.9 \times 10^{-1}$	$-4.8 \times 10^{-1}$	0.61	0.7	1996	[25–27]
2	<i>p</i> -Cl-TEMPO	Nitroxyl	0.28	$-2.7 \times 10^{-1}$	$-9.9 \times 10^{-1}$	0.28	0.6	2001	[30]
3	2,5-DFPNN	Nitroxyl	0.45	$+3.6 \times 10^{-1}$	$+7.9 \times 10^{-1}$	>0.57		2003	[28]
4	Dupeyredioxyl	Nitroxyl	1.48	$-5.0 \times 10^{-1}$	$-3.4 \times 10^{-1}$	1.48		2003	[29]
5	<i>p</i> -O <sub>2</sub> NC <sub>6</sub> F <sub>4</sub> CNSSN	Thiazyl	1.30	$+5.9 \times 10^{-1}$	$+4.5 \times 10^{-1}$	1.8		2005	[5]
6	$\gamma$ -BBDTA $\cdot$ GaCl <sub>4</sub>	Thiazyl	7.0	+5.1	$+7.3 \times 10^{-1}$	14.5		2008	[16]
7	ClBPSSEt	Selenazyl	17	+6.7	$+4.1 \times 10^{-1}$	22		2009	[20,31]
8	BrBPSSEt	Selenazyl	17	+1.1	$+6.2 \times 10^{-2}$	25		2011	[21]
9	IBPSSEt	Selenazyl	11	+8.7	$+7.9 \times 10^{-1}$	27.5		2016	[22]

as seen in Fig. 3(a). With a view to improving upon the accuracy of our ac measurements on these bisdiselenazolyls [20–22,31], and also the broader objective of assessing the high-pressure properties of future generations of organic radical ferromagnets, we have developed a technique for the measurement of dc susceptibility at high pressures using a vibrating-coil superconducting quantum interference device (SQUID) magnetometer. Herein we describe this technique

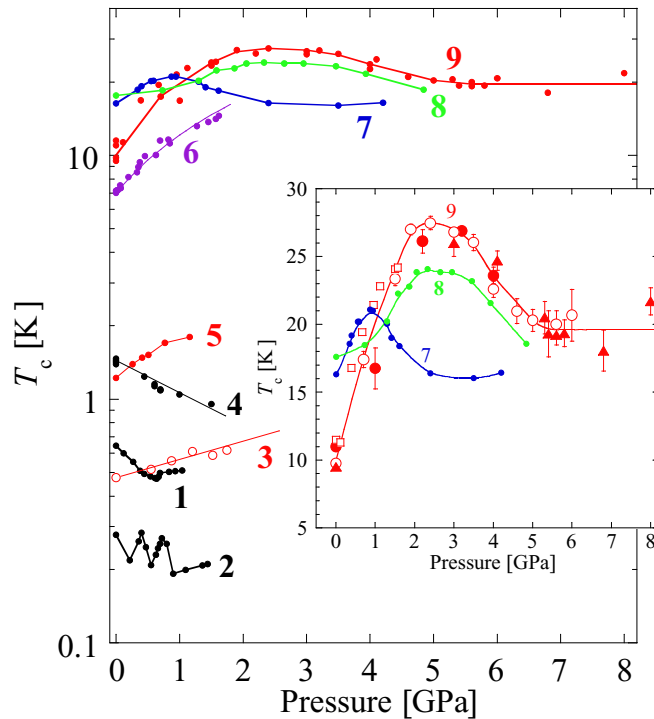


FIG. 1. Pressure dependence of  $T_C$  for representative radical ferromagnets; see Table I for the numbering scheme. The initial response of  $T_C$  to pressure for thiazyl and selenazyl radicals 5–9 is positive, contrary to that of nitroxyl radicals except for 3. The inset shows the detailed pressure dependence of  $T_C$  for the three bisdiselenazolyl radicals XBPSSEt ( $X = Cl, Br, I$ ) [20–22,31].

and demonstrate its use in the exploration of the high-pressure magnetic structure of IBPSSEt.

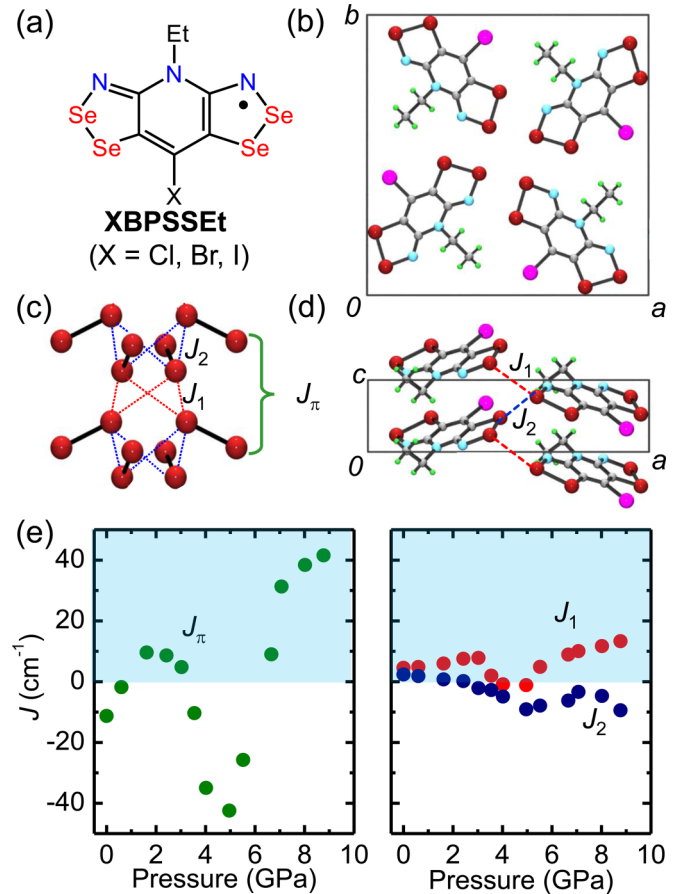


FIG. 2. (a) Molecular framework of bisdiselenazolyl radicals XBPSSEt ( $X = Cl, Br, I$ ). (b) Unit cell of IBPSSEt, space group  $P\bar{4}2_1m$ . (c), (d) Intermolecular magnetic exchange interactions around  $\bar{4}$  points ( $J_1, J_2$ ) and along  $\pi$  stacks ( $J_\pi$ ). (e) Variation in DFT-BS calculated magnetic exchange energies as a function of pressure,  $J_\pi$  in green,  $J_1$  in red, and  $J_2$  in blue [22]; ferromagnetic regions are highlighted in blue.

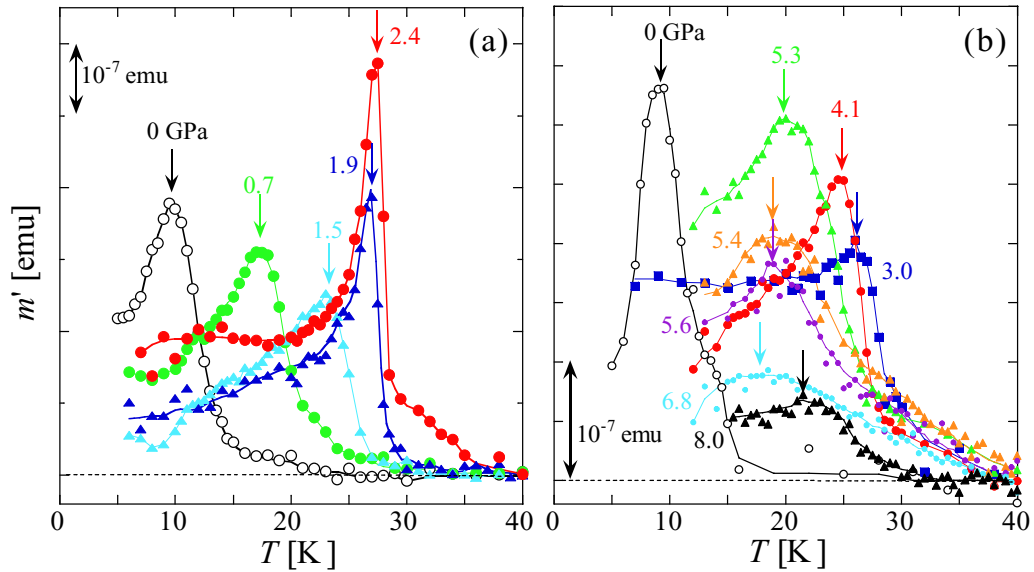


FIG. 3. Temperature dependence of the in-phase component  $m'$  of ac magnetic susceptibility measurement on IBPSSEt, using a miniature DAC and SQUID, performed over low-pressure [(a)  $P \leq 2.4$  GPa] and high-pressure [(b)  $P \leq 8.0$  GPa] ranges [22]. The out-of-phase component mainly reflects large ac magnetic responses due to the eddy current of DAC, and it is not useful to detect any magnetic signal of the target material.

## II. HIGH-PRESSURE MAGNETIC MEASUREMENTS FOR FERROMAGNETIC ORDER USING SQUID MAGNETOMETRY

The conventional method for the identification of ferromagnetic ordering involves measurement of field-cooled (FC) magnetization at a finite dc magnetic field ( $H_{dc}$ ). The electromagnetic induction type detects the magnetic dynamics. On the other hand, in a SQUID magnetometer, the magnetic flux passing the detection coil is converted into an output voltage ( $V$ ). Thus, the physical quantity observed by SQUID corresponds to the magnetization ( $M$ ) of the target material;  $M$  is proportional to both the specimen volume and  $H_{dc}$ . Herein we focus on the drift in  $V$ , which must be deleted in order to generate an accurate value of  $M$ .

The measurement of  $M$  at a finite  $H_{dc}$  under pressures up to approximately 10 GPa requires the use of diamond anvil cell (DAC) techniques. The key components of a DAC are two diamond anvils, with a gasket sandwiched between them [32]. The location of the magnetic detection coil is restricted because of the space limitations, as seen in Fig. 4(a). The valid techniques to solve the drift problem in this extremely confined geometry are restricted to (1) a Fourier analysis of the response  $V$  to an applied ac magnetic field  $H_{ac}$  (SQUID-ac) [20–22] resulting in ac magnetic susceptibility and (2) a Fourier analysis of  $V$  responding to axial vibration of the detection coil (vibrating-coil SQUID magnetometer, so-called SQUID-VCM) [33,34] resulting in dc magnetic susceptibility.

One approach similar to method (1) is to use a commercial SQUID magnetometer with a miniature DAC [35]. This is particularly useful for high-pressure experiments on cuprate superconductors because of the wide temperature range accessible [36–38]. In this approach, the detection coil, with an inside diameter of 20 mm, is located in the liquid-helium

bath, thermally isolated from the sample chamber. Here,  $V$  reflects the magnetic flux from the miniature DAC (both intrinsic magnetic and eddy-current induced magnetic fluxes) as well as  $M$  of the target sample.  $V$  is measured at the same frequency as that of  $H_{ac}$ . The smaller the moment of the sample becomes, the more difficult it is to distinguish from the background of the DAC itself.

Previous high-pressure experiments on IBPSSEt were conducted using ac magnetic susceptibility methods on a commercial SQUID magnetometer [22]; technical details are described elsewhere [31]. The amplitude of  $H_{ac}$  was 3.86 Oe. The magnetic signal became small and broad near  $P = 4$  GPa, as seen in Figs. 3(a) and 3(b). By contrast, in the SQUID-VCM experiment, the detection coil of 20 turns equipped with the compensation coil of 10 turns is slightly separated from the gasket and it effectively detects the magnetic flux of the target material. The  $V$  component oscillating with a frequency equal to that of the coil vibration is obtained by Fourier analysis. It is important to note that the detected signal is not a dynamic response but a static response to the coil movement in a fixed  $H_{dc}$ , representing the dc magnetic susceptibility.

## III. EXPERIMENTAL METHOD: SQUID-VCM

The synthesis of IBPSSEt (8-iodo-4-ethyl-4H-bis[1,2,3]diselenazolo[4,5-*b*:5',4'-*e*]pyridin-3-yl) has been described elsewhere [22]. Samples were sealed in glass vials under vacuum until sample preparation for the high-pressure experiment. The DFT broken symmetry calculated  $J$  values cited herein [22] are defined in magnitude and sign in terms of the phenomenological Hamiltonian  $H_{ex} = -2J_{ij}\{S_i \cdot S_j\}$ .

The DAC is mounted in the  $^4\text{He}$  refrigerator with a 1-K pot, and the entire DAC is heated. The use of diamond anvils with different culet sizes (i.e., 500 and 550  $\mu\text{m}$ ) allows the

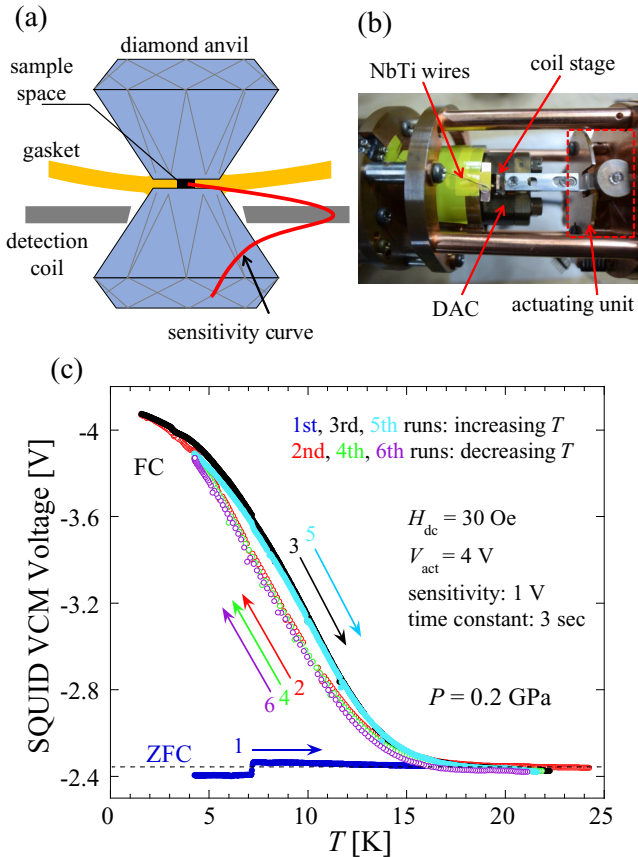


FIG. 4. (a) Overview of SQUID-VCM: The use of diamond anvils with different culet size (i.e., 500 and 550  $\mu\text{m}$ ) allows the CuBe-NiCrAl composite gasket to be deformed away from the NbTi detection coil. The detection coil is ideally vibrated at the place where the slope of magnetic flux against the distance from the sample (shown as the sensitivity curve) is maximum. (b) Photograph of the DAC and actuating unit in the cryostat. (c) An example of a performance test for IBPSSEt at  $P = 0.2$  GPa: It contains one heating process after ZFC, three field-cooling (FC) ones, and two heating ones after FC. By investigating the influence of field cooling, the development of ferromagnetic correlation can be observed.

CuBe-NiCrAl composite gasket to be deformed away from the NbTi detection coil. The NiCrAl disk with a diameter of 410  $\mu\text{m}$  was inserted into the hole drilled in the center of the CuBe gasket [39]. After pressing the composite gasket down to 70  $\mu\text{m}$ , a hole with a diameter of 200  $\mu\text{m}$  was drilled in the center. In the sample cavity, the powdered sample of IBPSSEt was held together with the pressure transmitting medium (PTM) Apiezon-J oil or Daphne oil 7373, ruby as a room-temperature manometer, and lead as a manometer at liquid- $^4\text{He}$  temperature. The magnitude of the pressure ( $P$ ) was estimated at room temperature by measuring the fluorescence of ruby [40]. Using an actuating unit consisting of three piezoelectric actuators of bimorph type, the detection coil is ideally vibrated at the place where the slope of magnetic flux against the distance from the sample is maximum, as shown in Fig. 4(a). To obtain sufficient amplitude of the vibration of the detection coil at liquid-helium temperature, the driving frequency of the vibrating actuators is chosen to be 168 Hz, that is, near

the resonating frequency of the vibrating actuators. The DAC and the actuating unit are located in the cryostat, as shown in Fig. 4(b). Consequently,  $V$  is a sinusoidal function with the above frequency, and  $V$  increases along with  $H_{\text{dc}}$ .  $H_{\text{dc}}$  was applied at 30 Oe at maximum. The use of a lock-in amplifier at the vibration frequency yields the amplitude of  $V$ . Figure 4(c) shows the temperature dependence of  $V$  for IBPSSEt at  $P = 0.2$  GPa. In the initial zero-field-cooled (ZFC) measurement, the Meissner signal of lead is larger than the magnetically positive response of IBPSSEt above 15 K. During subsequent field-cooled measurements, while maintaining  $H_{\text{dc}}$  of 30 Oe, the sample was repeatedly warmed and cooled. While a small thermal hysteresis is noted, the temperature below which  $M$  exhibits a prominent increase does not change. Using this increase as its definition,  $T_{\text{C}}$  becomes 15 K. It is stressed that there is a large enhancement on field cooling, characteristic of FM ordering, making this technique suitable for high-pressure measurements of ferromagnets [41].

#### IV. EXPERIMENTAL RESULTS

Figure 5 shows the  $M$ - $T$  profile for IBPSSEt performed over two runs at 30 Oe, the first [Fig. 5(a)] using Apiezon-J oil as the PTM and the second [Fig. 5(b)] using Daphne oil 7373 as the PTM. Figure 5(a) presents the data for  $P = 0, 2.1, \text{ and } 4.1$  GPa cycled through cooling and heating after FC. At  $P = 0$  GPa, there is a small hysteresis between the two cycles; indeed, at all three pressures, a slight hysteresis was observed. Figure 5(b) shows the heating cycle data for  $P = 0.2, 3.7, 6.3, \text{ and } 9.7$  GPa after FC.

With reference to the heating curves, the value of  $M$  at  $P = 0$  GPa gradually changes below 17 K, and  $M$  increases rapidly for  $T < 13$  K. However, at  $P = 2.1$  GPa, there is an abrupt increase rather than a gradual change in  $M$  near  $T_{\text{C}} = 27.5$  K, exhibiting an ideal ferromagnetic  $T$  dependence of  $M$ . The ferromagnetic curvature of  $M(T)$  was also observed at 3.7 GPa in the second run. However, as  $P$  increases as  $P = 2.1 \rightarrow 3.7 \rightarrow 4.1 \rightarrow 6.3$  GPa,  $M$  decreases systematically. For  $P = 0, 2.1, \text{ and } 3.7$  GPa, the lead manometer exhibits an inverse Meissner signal, as seen in the inset of Fig. 5 for  $P = 2.1$  GPa, in response to the FM order of IBPSSEt. On the other hand, for  $P \geq 4.1$  GPa, the lead exhibits a normal Meissner signal. It is considered that the regular FM ordering collapses at approximately 4 GPa. The  $M$  for  $P \geq 4.1$  GPa was prominently observed in the FC process. There, the ferromagnetic domains should exist, and a certain exchange path changes the sign from positive (ferromagnetic) to negative (antiferromagnetic). As seen in the inset of Fig. 5(b),  $M$  for  $P = 6.3$  and 9.7 GPa increases in two steps, suggesting the existence of at least two dominant exchange paths.

The  $T$  dependence of  $M$  at  $P = 2.1$  GPa is typical for FM order predicted by mean-field theory. The two solid and two dashed curves in Fig. 6(a) stand for the Brillouin function with  $S = 1/2$  and  $T_{\text{C}} = 25.0, 26.0, 27.0, \text{ and } 27.5$  K. Given the inevitable pressure distribution of approximately 10% expected in the highly compressed state, we conclude that the  $M(T)$  curve at  $P = 2.1$  GPa is well reproduced with the Brillouin function. In particular,  $M(T)$  observed in the warming process can be reproduced with  $T_{\text{C}} = 27.0\text{--}27.5$  K. We try to reproduce the increase in  $M$  at  $H_{\text{dc}} = 30$  Oe just below  $T_{\text{C}}$  by using

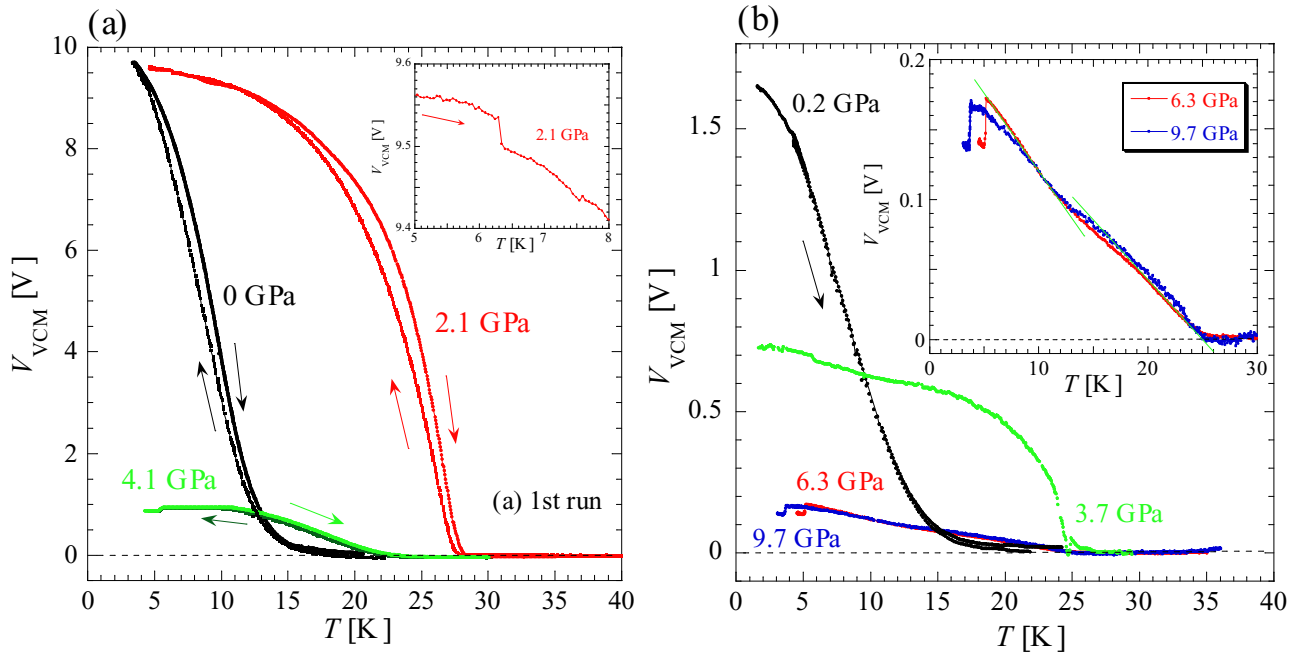


FIG. 5. SQUID-VCM measurement for IBPSSEt using (a) Apiezon-J oil as the PTM for both the FC process of 30 Oe and heating process maintaining its  $H_{dc}$  and (b) Daphne oil 7373 as the PTM for the heating process after FC of 30 Oe. The insets of (a) and (b) show  $M(T)$  for the heating process at (a)  $P = 2.1$  GPa and (b)  $P = 6.3$  and 9.7 GPa, respectively.

the scaling curve of  $(T_C - T)^\beta$  for the spontaneous magnetization. Now it is difficult to estimate the critical exponent from the log-log plot of  $M(T)$  for  $T < T_C$  due to the inevitable pressure distribution and temperature gradient. When looking at  $M(T)$  over a wide  $T$  range as shown in Fig. 6(b), the growth of  $M$  below  $T_C$  can be reproduced by the scaling curve with the critical exponent  $\beta = 0.369$  in the three-dimensional Heisenberg system [42] and  $T_C = 26.0\text{--}28.0$  K. We conclude that an ideal three-dimensional FM order with an isotropic nature is stabilized there, and further confirm  $T_C$  is the highest one among those observed for an organic system.

Figure 7 shows the  $P$  dependence of  $T_C$  for IBPSSEt, along with the results obtained previously from SQUID-ac measurements [22]. In the latter  $T_C$  was determined as  $T$  corresponding to the peak position of ac magnetization  $M_{ac}$  as seen in Fig. 3. However, in the present dc susceptibility measurements  $M_{dc}$ ,  $T_C$  represents  $T$  exhibiting the prominent increase of  $M$ . Below 4 GPa,  $T_C$ 's obtained by the two methods are satisfyingly consistent, both displaying a maximum near 2 GPa. Above 4 GPa, there is a broad anomaly in  $M_{ac}$ , where the peak temperature hardly changes with pressure. However,  $M_{dc}$  has a two-stage increase, suggesting that the magnetic ordering proceeds in two steps with decreasing  $T$ .

## V. DISCUSSION

As illustrated in Fig. 2, the magnetic structure of IBPSSEt possesses both axial ( $J_\pi$ ) and lateral ( $J_{1,2}$ ) exchange pathways, and DFT calculations suggest that the axial  $J_\pi$  interaction should become more ferromagnetic with increasing

pressure, so that around 1.5–2.0 GPa all exchange pathways are FM ( $+ve$ ) in nature. This would correspond to the optimal ferromagnetic state identified by the  $M_{dc}$  measurements, as seen in Fig. 6. Above this optimal pressure, all three exchange interactions ( $J_\pi$  and  $J_{1,2}$ ) trend towards antiferromagnetic ( $-ve$ ) values. Indeed,  $M_{dc}$  shifts slightly toward lower temperature (Fig. 5), and its maximum value is reduced. At  $P > 3$  GPa  $J_2$  continues to decrease to more AFM values, but both  $J_\pi$  and  $J_1$  start to increase at around 4–5 GPa, and beyond 6 GPa  $J_\pi$  in particular experiences a large FM enhancement, which arises from a decrease in the degree of slippage of the radical  $\pi$ -stacks [22]. As a result, the magnetic network may be considered to be a one-dimensional (1D) axial FM system with weak FM  $J_1$  and weak AFM  $J_2$  lateral interactions. From the viewpoint of the dimensionality of the magnetic structure, the spin system changes to being predominantly 2D at  $P < 1.5$  GPa to 3D near  $P = 2$  GPa to 1D at  $P > 6$  GPa. As illustrated in Fig. 7, the upper characteristic temperature observed at  $P = 6.3$  and 9.7 GPa is related with the 1D FM exchange path as dominant exchange contributor, while the lower one originates primarily from the interchain interactions consisting of FM ( $J_1$ ) and AFM ( $J_2$ ) paths.

## VI. CONCLUSION

We have investigated the variable pressure response of the field-cooled magnetization  $M_{dc}$  of the neutral radical ferromagnet IBPSSEt using SQUID-VCM methods. Analysis of the results has provided insight into the dominant magnetic interaction paths that contribute to the overall magnetic structure. At ambient pressure, the magnetic structure is

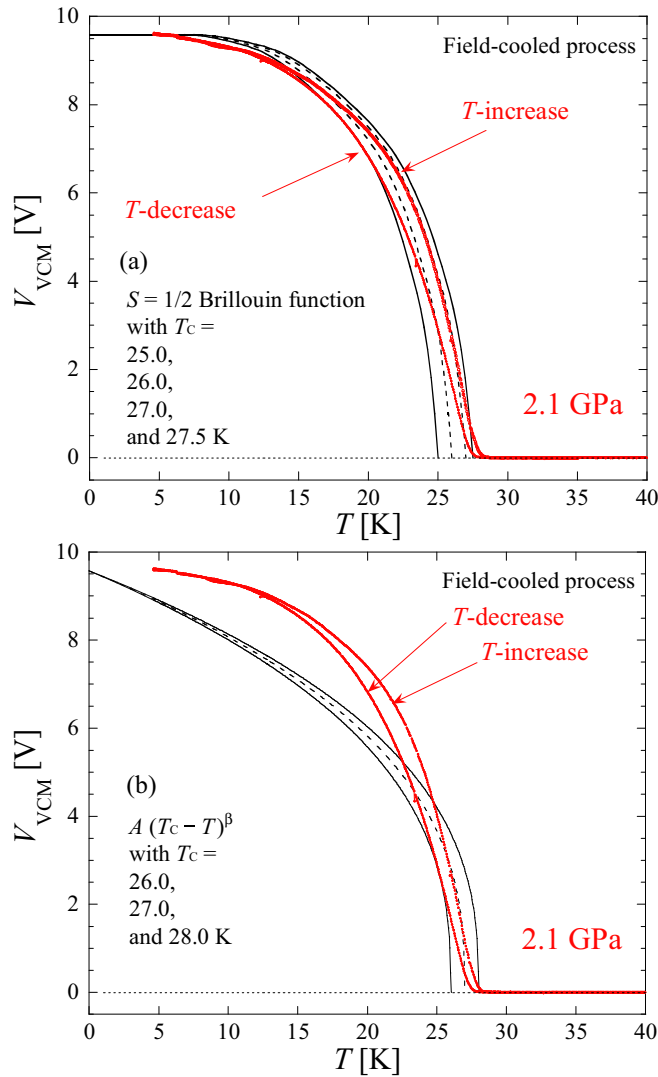


FIG. 6. The analyses of  $M(T)$  for both a  $T$  decrease and  $T$  increase in the FC process at  $P = 2.1$  GPa using the Brillouin function (a) and scaling curve with critical component ( $\beta = 0.369$ ) for the spontaneous magnetization in the three-dimensional Heisenberg system (b). In (a),  $M(T)$  observed in the warming process can be reproduced with the Brillouin function with a spin quantum number  $S = 1/2$  and  $T_c = 27.0\text{--}27.5$  K. In (b), there are three scaling curves proportional to  $(T_c - T)^\beta$  with  $\beta = 0.369$  and  $T_c = 26.0\text{--}28.0$  K.  $A$  is an arbitrary constant.

dominated by lateral (2D) exchange interactions, but with compression, enhanced exchange interactions along the  $\pi$

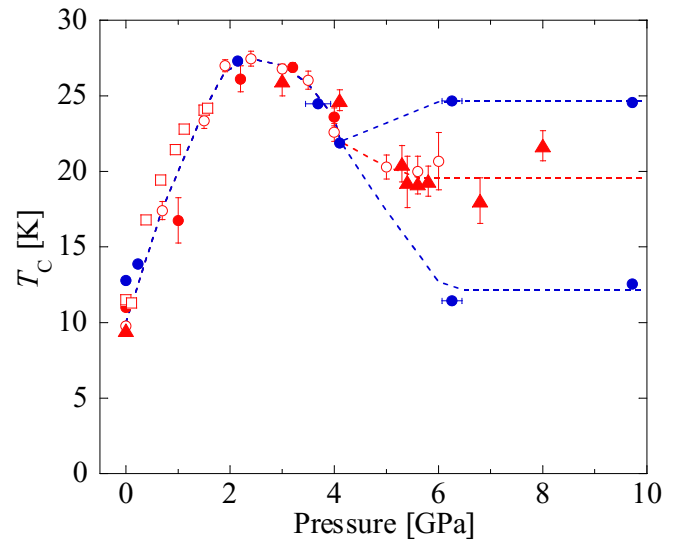


FIG. 7. Pressure dependence of Curie temperature  $T_c$  for IBPS-SEt; solid blue circles stand for the characteristic temperature estimated in the dc measurements, which corresponds to  $T_c$  for  $P < 4.1$  GPa. For  $P > 6$  GPa, there are two characteristic temperatures. For reference, red symbols present the results of the ac measurements by piston cylinder cell ( $\square$ ) and DAC ( $\circ, \bullet, \blacktriangle$ ) [22].

stacks ( $J_\pi$ ) give rise to a more isotropic 3D FM network. In particular, we have been able to confirm experimentally that the state at 2 GPa is the ideal FM system, and its  $T_c = 27.5$  K is the highest one among organic spin systems. With further compression, the magnetic structure becomes dominated by the value of  $J_\pi$ , so that at  $P > 6$  GPa the material may be considered as a 1D FM chain system. The present study thus demonstrates how accurate  $M_{\text{dc}}$  measurements may be used in conjunction with high-pressure powder x-ray diffraction data and DFT calculations to understand subtle pressure-driven changes in the dimensionality of the magnetic networks within organic ferromagnets.

#### ACKNOWLEDGMENT

This work was supported by Grants-in-Aid for Scientific Research, Grants No. (B) 26289091 and No. 17H03379, from the Ministry of Education, Culture, Sports, Science and Technology (MEXT), Japan, and by the Natural Sciences and Engineering Research Council of Canada (NSERCC).

[1] P. W. Anderson, *Concepts in Solids* (W. A. Benjamin, New York, 1963), p. 7.  
 [2] J. S. Miller, *Adv. Mater.* **14**, 1105 (2002).  
 [3] S. J. Blundell and F. L. Pratt, *J. Phys.: Condens. Matter* **16**, R771 (2004).  
 [4] *Molecular Magnetism: New Magnetic Materials*, edited by K. Itoh and M. Kinoshita (Gordon and Breach, New York, 2000).  
 [5] *Carbon-Based Magnetism*, edited by T. Makarova and F. Palacio (Elsevier, Amsterdam, 2005).

[6] S. M. Winter, S. Hill, and R. T. Oakley, *J. Am. Chem. Soc.* **137**, 3720 (2015).  
 [7] K. Mukai, H. Nishiguchi, and Y. Deguchi, *J. Phys. Soc. Jpn.* **23**, 125 (1967).  
 [8] K. Mukai, H. Nishiguchi, and Y. Deguchi, *Bull. Chem. Soc. Jpn.* **42**, 40 (1969).  
 [9] M. Kinoshita, P. Turek, M. Tamura, K. Nozawa, D. Shiomi, Y. Nakazawa, M. Ishikawa, M. Takahashi, K. Awaga, T. Inabe *et al.*, *Chem. Lett.* **20**, 1225 (1991).

- [10] R. Chiarelli, M. A. Novak, A. Rassat, and J. L. Tholence, *Nature (London)* **363**, 147 (1993).
- [11] T. Sugawara, M. Matushita, A. Izuoka, N. Wada, N. Takeda, and M. Ishikawa, *J. Chem. Soc., Chem. Commun.* **1723** (1994).
- [12] T. Nogami, T. Ishida, H. Tsuboi, H. Yoshikawa, H. Yamamoto, M. Yasui, F. Iwasaki, H. Iwamura, N. Takeda, and M. Ishikawa, *Chem. Lett.* **24**, 635 (1995).
- [13] S. Nakatsuji, H. Morimoto, H. Anzai, J. Kawashima, K. Maeda, M. Mito, and K. Takeda, *Chem. Phys. Lett.* **296**, 159 (1998).
- [14] J. Banister, N. Bricklebank, I. Lavender, J. M. Rawson, C. I. Gregory, B. K. Tanner, M. R. J. E. W. Clegg, and F. Palacio, *Angew. Chem., Int. Ed. Engl.* **35**, 2533 (1996).
- [15] W. Fujita and K. Awaga, *Chem. Phys. Lett.* **388**, 186 (2004).
- [16] M. Mito, M. Fujino, Y. Komorida, H. Deguchi, S. Takagi, W. Fujita, and K. Awaga, *J. Phys. Soc. Jpn.* **77**, 124713 (2008).
- [17] C. M. Robertson, D. J. T. Myles, A. A. Leitch, R. W. Reed, B. M. Dooley, N. L. Frank, P. A. Dube, L. K. Thompson, and R. T. Oakley, *J. Am. Chem. Soc.* **129**, 12688 (2007).
- [18] C. M. Robertson, A. A. Leitch, K. Cvrkalj, R. W. Reed, D. J. T. Myles, P. A. Dube, and R. T. Oakley, *J. Am. Chem. Soc.* **130**, 8414 (2008).
- [19] P. M. Allemand, K. C. Khemani, A. Koch, F. Wudl, K. Holczer, S. Donovan, G. Gruner, and J. D. Thompson, *Science* **253**, 301 (1991).
- [20] M. Mito, Y. Komorida, H. Tsuruda, J. S. Tse, S. Desgreniers, Y. Ohishi, A. A. Leitch, K. Cvrkalj, C. M. Robertson, and R. T. Oakley, *J. Am. Chem. Soc.* **131**, 16012 (2009).
- [21] A. A. Leitch, K. Lekin, S. M. Winter, L. E. Downie, H. Tsuruda, J. S. Tse, M. Mito, S. Desgreniers, P. A. Dube, S. Zhang *et al.*, *J. Am. Chem. Soc.* **133**, 6051 (2011).
- [22] K. Lekin, K. Ogata, A. Maclean, A. Mailman, S. M. Winter, A. Assoud, M. Mito, J. S. Tse, S. Desgreniers, N. Hirao *et al.*, *Chem. Commun.* **52**, 13877 (2016).
- [23] Y. Hosokoshi, M. Tamura, and M. Kinoshita, *Mol. Cryst. Liq. Cryst.* **306**, 423 (1997).
- [24] Y. Hosokoshi, M. Mito, M. Tamura, K. Takeda, K. Inoue, and M. Kinoshita, *Rev. High Pressure Sci. Technol.* **7**, 620 (1998).
- [25] K. Takeda, K. Konishi, M. Tamura, and M. Kinoshita, *Phys. Rev. B* **53**, 3374 (1996).
- [26] M. Mito, T. Kawae, M. Takumi, K. Nagata, M. Tamura, M. Kinoshita, and K. Takeda, *Phys. Rev. B* **56**, R14255 (1997).
- [27] K. Takeda, M. Mito, T. Kawae, M. Takumi, K. Nagata, M. Tamura, and M. Kinoshita, *J. Phys. Chem. B* **102**, 671 (1998).
- [28] M. Mito, H. Deguchi, T. Tanimoto, T. Kawae, S. Nakatsuji, H. Morimoto, H. Anzai, H. Nakao, Y. Murakami, and K. Takeda, *Phys. Rev. B* **67**, 024427 (2003).
- [29] K. Takeda, M. Mito, K. Kinoshita, M. Novak, J. Tholence, and A. Rassat, *Polyhedron* **22**, 2287 (2003).
- [30] M. Mito, T. Kawae, M. Hitaka, K. Takeda, T. Ishida, and T. Nogami, *Chem. Phys. Lett.* **333**, 69 (2001).
- [31] H. Tsuruda, M. Mito, H. Deguchi, S. Takagi, A. A. Leitch, K. Lekin, S. M. Winter, and R. T. Oakley, *Polyhedron* **30**, 2997 (2011).
- [32] M. Eremets, *High Pressure Experimental Methods* (Oxford University Press, New York, 1996).
- [33] M. Ishizuka, K. Amaya, and S. Endo, *Rev. Sci. Instrum.* **66**, 3307 (1995).
- [34] J. Yamada, K. Irie, M. Mito, H. Deguchi, and S. Takagi, *J. Magn. Magn. Mater.* **310**, 2734 (2007).
- [35] M. Mito, M. Hitaka, T. Kawae, K. Takeda, T. Kitai, and N. Toyoshima, *Jpn. J. Appl. Phys.* **40**, 6641 (2001).
- [36] M. Mito, T. Imakyurei, H. Deguchi, K. Matsumoto, H. Hara, T. Ozaki, H. Takeya, and Y. Takano, *J. Phys. Soc. Jpn.* **83**, 023705 (2014).
- [37] M. Mito, H. Matsui, H. Goto, H. Deguchi, K. Matsumoto, H. Hara, T. Ozaki, H. Takeya, and Y. Takano, *J. Phys. Soc. Jpn.* **85**, 024711 (2016).
- [38] M. Mito, K. Ogata, H. Goto, K. Tsuruta, K. Nakamura, H. Deguchi, T. Horide, K. Matsumoto, T. Tajiri, H. Hara *et al.*, *Phys. Rev. B* **95**, 064503 (2017).
- [39] M. Ishizuka, *Rev. Sci. Instrum.* **76**, 123902 (2005).
- [40] G. J. Piermarini, S. Block, J. D. Barnett, and R. A. Forman, *J. Appl. Phys.* **46**, 2774 (1975).
- [41] M. Abdel-Hafiez, M. Mito, K. Shibayama, S. Takagi, M. Ishizuka, A. N. Vasiliev, C. Krellner, and H. K. Mao, *Phys. Rev. B* **98**, 094504 (2018).
- [42] M. Camprostrini, M. Hasenbusch, A. Pelissetto, P. Rossi, and E. Vicari, *Phys. Rev. B* **65**, 144520 (2002).